J. Iran. Chem. Soc., Vol. 7, No. 3, September 2010, pp. 707-720.

JOURNAL OF THE
Iranian
Chemical Society

Synthesis and Characterization of Three Organic Dyes with Various Donors and Rhodanine Ring Acceptor for Use in Dye-Sensitized Solar Cells

T.Y. Wu[a], M.H. Tsao[a], F.L. Chen[a], S.G. Su[a], C.W. Chang[a], H.P. Wang[b,c], Y.C. Lin[d] and I.W. Sun[a,b]*

[a]*Department of Chemistry, National Cheng Kung University, Tainan, Taiwan*

[b]*Sustainable Environment Research Center, National Cheng Kung University, Tainan 701, Taiwan*

[c]*Department of Environmental Engineering, National Cheng Kung University, Tainan, Taiwan*

[d]*Institute of Environmental Engineering, National Sun Yat-Sen University, Kaohsiung 804, Taiwan*

(Received 22 August 2009, Accepted 29 October 2009)

A series of new organic dyes comprising carbazole, iminodibenzyl, and phenothiazine moieties as the electron donors and rhodanine ring as the electron acceptor/anchoring groups were designed and developed for use in dye-sensitized solar cells. HOMO and LUMO energy level tuning was achieved by varying the carbazole, iminodibenzyls and phenothiazine donors. This was evidenced by spectral and electrochemical experiments and density functional theory calculations. Electrochemical studies indicated that the phenothiazine unit was much more effective in lowering the ionization potential than were the iminodibenzyl and carbazole units. The phenothiazine dye shows a solar-energy-to-electricity conversion efficiency (η) of 4.87%; the carbazole and iminodibenzyl dyes show η of 2.54% and 3.52%, respectively. These findings reveal that using carbazole, iminodibenzyl and phenothiazine donors as light-harvesting sensitizers are promising candidates for dye-sensitized solar cells.

Keywords: Dye-sensitized solar cells, Organic dyes, Donor, Absorption, Electrochemistry, Rhodanine

INTRODUCTION

The growing demand for energy and global warming necessitate a greater focus on renewable energy sources. A dye-sensitized solar cell (DSSC) using Ru complexes as a photosensitizer was first reported by O'Regan and Grätzel in 1991 [1]. Its low-cost and easy preparation makes DSSC one of the most promising photovoltaic cells. Ruthenium polypyridyl complexes are the most promising sensitizers for DSSCs, achieving power conversion efficiencies (η) >10% [2] and good long-term stability [3]. Although the most efficient sensitizers to date are ruthenium complexes, organic dyes have been attracting attention because of their ease of synthesis, high molar extinction coefficient, tunable absorption spectral response from the visible to the near infrared (NIR) region, environmental friendliness and inexpensive production techniques. Since 2000 AD, an increasing number of studies have been devoted to the development of organic dyes [4-7]. Reasonable photoconversion efficiencies have been reached with some push-pull type organic chromophores [8]. Recently, some organic coumarin [9], indoline [10], merocyanine [11] and hemicyanine dyes [12] have shown impressive photovoltaic performance. Most of the organic sensitizers applied in DSSC act as both the electron donors (D) and the electron acceptors (A) linked by a π-conjugation bridge, which is called the D-π-A structure [13]. However, many organic dyes exhibit low conversion efficiency in DSSCs due to the formation of dye aggregates on the semiconductor surface.

*Corresponding author. E-mail: iwsun@mail.ncku.edu.tw

They are also associated with low operational stability due to the formation of unstable radical species during redox reaction cycles. Organic dyes have a push-pull structure similar to that of nonlinear optical molecules, which are composed of a donor, conjugated bridge, and acceptor. Many researchers have attempted to create organic dyes through the structural modification of the donor [14], conjugated bridge [15], or acceptor unit [16]. Thus, we are interested in the structural modification of the organic dyes' donor unit to develop efficient organic dyes which would not aggregate. Our second objective is to study the effect of such structural changes on DSSC efficiency.

Iminodibenzyl is a diphenylamine wherein two *ortho* positions are joined by a dimethylene bridge. For phenothiazine sensitizer, the two *ortho* positions of the diphenylamine are joined by an electron-donating sulfur atom. No DSSC dyes with iminodibenzyl sensitizers have been reported. Phenothiazine sensitizer is incorporated in this study in order to compare the structure impact between dimethylene bridge and sulfur atom. In this work, metal-free dyes with carbazole, iminodibenzyl, and phenothiazine sensitizers are reported and their optical, electrochemical, photovoltaic properties and structural relationships are investigated in detail.

EXPERIMENTAL

Chemicals

All starting materials were purchased from Aldrich (St. Louis Missouri), Lancaster (Karlsruhe), TCI (Tokyo), and Acros (Geel) and used as received. Dimethylformamide (DMF), dichloromethane, and $POCl_3$ were distilled over CaH_2 under N_2 atmosphere. Tetrabutylammonium perchlorate (TBAP) was purchased from Alfa Aesar (Karlsruhe), and 1,2-dimethyl-3-propylimidazolium iodide (DMPImI) was synthesized and purified according to a procedure in the literature [17].

Synthetic Procedure for Carbazole, Iminodibenzyl, and Phenothiazine-Containing Dyes (R1-R3)

11-Ethyl-iminodibenzyl (2b). Iminodibenzyl (**1b**: 6.834 g, 35 mmol), iodoethane (5.93 g, 38 mmol), and 80 ml of DMF were added to a 50-ml two-necked glass reactor. The solution was warmed to 75 °C, treated portionwise with potassium *tert*-butoxide (4.264 g, 38 mmol), and then refluxed for 24 h. After 150 ml of water was added, the mixture was extracted with chloroform (75 ml). Crude oils obtained by removing the solvent were purified by column chromatography (silica gels, *n*-hexane/ethyl acetate: 20/1 as eluent) to give **2b** as a white solid (4.76 g, 61%). ^{1}H NMR ($CDCl_3$), δ (ppm): 1.16 (t, 3H, CH_3), 3.17 (m, 4H, CH_2), 3.80 (m, 2H, CH_2), 6.92 (m, 2H, ar), 7.12 (m, 6H, ar). Elem. Anal. Calcd. for $C_{16}H_{17}N$: C, 86.05%; H, 7.67%; N, 6.27%. Found: C, 85.96%; H, 7.73%; N, 6.20%.

11-Ethyl-3-formyliminodibenzyl (3b). $POCl_3$ (7.4 g, 48 mol) was added dropwise to 4.3 g (58 mmol) of freshly distilled *N*,*N*-dimethylformamide at 0 °C in nitrogen atmosphere. A solution of 11-ethyl-iminodibenzyl (**2b**: 3.35 g, 15 mmol) in *N,N*-dimethylformamide was added dropwise to $POCl_3$/DMF complex at 30 °C. The reaction mixture was stirred at 80 °C for 4 h. When the reaction finished (TLC monitoring), the reaction mixture was cooled to room temperature and poured into ice water. The obtained mixture was neutralized with NaOH until pH = 7-8. The precipitates were separated by filtration and washed with methanol. The crude product was purified by column chromatography (eluent:ethylacetate-hexane, 1:6). Yield of **3b**: 3.2 g (85%). ^{1}H NMR ($CDCl_3$), δ (ppm): 1.07 (t, 3H, CH_3), 3.11 (m, 4H, CH_2), 3.85 (m, 2H, CH_2), 7.00-7.08 (m, 1H, ar), 7.19-7.28 (m, 4H, ar), 7.57 (s, 1H, ar), 7.64-7.67 (m, 1H, ar), 9.78 (s, 1H, CHO). Elem. Anal. Calcd. for $C_{17}H_{17}NO$: C, 81.24%; H, 6.82%; N, 5.57%. Found: C, 81.04%; H, 6.90%; N, 5.46%.

2-(5-((11-Ethyl-iminodibenzyl-2-yl)methylene)-4-oxo-2-thioxothiazolidin-3-yl)acetic acid (R2). To a stirred **3b** (1.005 g, 4 mmol) in CH_3COOH (30 ml) were added rhodanine-3-acetic acid (0.794 g, 4.15 mmol) and ammonium acetate (0.125 g, 1.625 mmol). Then the mixture was heated to 120 °C and the reaction continued for 2 h at the said temperature. Then the reaction mixture was allowed to cool to room temperature. The solid was collected by filtration and washed with water thoroughly. After drying in air, the crude product was purified by column chromatography on silica gel with CH_2Cl_2/methanol (10:1, v/v) as eluent to give **R2** in 83% yield. ^{1}H NMR ($CDCl_3$), δ (ppm): 1.08 (t, 3H, CH_3), 3.11 (m, 4H, CH_2), 3.86 (m, 2H, CH_2), 4.73 (s, 2H, CH_2), 7.04 (m, 1H), 7.19-7.28 (m, 4H), 7.36 (s, 1H), 7.45 (d, 1H), 7.74 (s, 1H).

Elem. Anal. Calcd. for $C_{22}H_{20}N_2O_3S_2$: C, 62.24%; H, 4.75%; N, 6.60%; S, 15.11%. Found: C, 62.14%; H, 4.72%; N, 6.58%; S, 15.02%.

10-Ethyl-phenothiazine (2c). Phenothiazine (**1c**: 11.94 g, 60 mmol), iodoethane (10.92 g, 70 mmol), and 80 ml of DMF were added to a 50-ml two-necked glass reactor. The solution was warmed to 75 °C, treated portionwise with potassium *tert*-butoxide (7.86 g, 70 mmol), and then refluxed for 24 h. After 150 ml of water was added, the mixture was extracted with chloroform (75 ml). Crude oils obtained by removing the solvent were purified by column chromatography (silica gels, *n*-hexane/ethyl acetate: 20/1 as eluent) to give **2c** as a white solid (11.32 g, yield: 83%). MP: 103-104 °C. ^{1}H NMR ($CDCl_3$), δ (ppm): 1.42 (t, 3H, CH_3), 3.92 (m, 2H, CH_2), 6.85-6.88 (m, 4H, ar), 7.11-7.16 (m, 4H, ar). Elem. Anal. Calcd. for $C_{14}H_{13}NS$: C, 73.97%; H, 5.76%; N, 6.16%; S, 14.11%. Found: C, 73.83%; H, 5.73%; N, 6.13%, S: 14.10%.

10-Ethyl-3-formylphenothiazine (3c). $POCl_3$ (14.8 g, 0.097 mol) was added dropwise to 8.6 g (0.116 mol) of freshly distilled *N*,*N*-dimethylformamide (molar ratio 1:1.2) at 0 °C in nitrogen atmosphere. A solution of 6.8 g (0.03 mol) of N-ethyl-phenothiazine in *N,N*-dimethylformamide was added dropwise to $POCl_3$/DMF complex at 30 °C. The reaction mixture was stirred at 80 °C for 4 h. When the reaction finished (TLC monitoring), the reaction mixture was cooled to room temperature and poured into ice water. The obtained mixture was neutralized with NaOH until pH = 7-8. The precipitates were separated by filtration and washed with methanol. The crude product was purified by column chromatography (eluent:ethylacetate-hexane, 1:6). Yield of **3c**: 5.36 g (70%). ^{1}H NMR ($CDCl_3$), δ (ppm): 1.45 (t, 3H, CH_3), 3.98 (m, 2H, CH_2), 6.88-6.98 (m, 3H, ar), 7.09-7.19 (m, 2H, ar), 7.57-7.65 (m, 2H, ar), 9.80 (s, 1H, CHO). Elem. Anal. Calcd. for $C_{15}H_{13}NOS$: C, 70.56%; H, 5.13%; N, 5.49%, S, 12.56%. Found: C, 70.49%; H, 5.26%; N, 5.37%, S, 12.38%.

2-(5-((10-Ethyl-phenothiazin-3-yl)methylene)-4-oxo-2-thioxothiazolidin-3-yl) acetic acid (R3). To a stirred **3c** (1.021 g, 4 mmol) in CH_3COOH (30 ml) were added rhodanine-3-acetic acid (0.794 g, 4.15 mmol) and ammonium acetate (0.125 g, 1.625 mmol). Then the mixture was heated to 120 °C and the reaction continued for 2 h at the said temperature. Then the reaction mixture was allowed to cool to room temperature. The solid was collected by filtration and washed with water thoroughly. After drying in air, the crude product was purified by column chromatography on silica gel with CH_2Cl_2/methanol (10:1, v/v) as eluant to give **R3** in 89% yield. ^{1}H NMR (DMSO-d_6), δ (ppm): 1.33 (t, 3H, CH_3), 3.99 (m, 2H), 4.73 (s, 2H), 6.97-7.25 (m, 5H), 7.40 (s, 1H), 7.49 (d, 1H), 7.78 (s, 1H). Elem. Anal. Calcd. for $C_{20}H_{16}N_2O_3S_3$: C, 56.05%; H, 3.76%; N, 6.54%, S, 22.45%. Found: C, 55.90%; H, 3.76%; N, 6.52%, S, 22.37%.

2-(5-((9-Ethyl-carbazol-3-yl)methylene)-4-oxo-2-thioxothiazolidin-3-yl) acetic acid (R1). 9-Ethyl-carbazole (**2a**) and 9-ethyl-3-formylcarbazole (**3a**) were synthesized following the procedures used for compounds **2b** and **3b**, respectively. To a stirred **3a** (0.893 g, 4 mmol) in CH_3COOH (30 ml) were added rhodanine-3-acetic acid (0.794 g, 4.15 mmol) and ammonium acetate (0.125 g, 1.625 mmol). Then the mixture was heated to 120 °C and the reaction continued for 2 h at the said temperature. Then the reaction mixture was allowed to cool to room temperature. The solid was collected by filtration and washed with water thoroughly. After drying in air, the crude product was purified by column chromatography on silica gel with CH_2Cl_2/ methanol (10:1, v/v) as eluant to give **R1** in 95% yield. ^{1}H NMR ($CDCl_3$), δ (ppm): 1.35 (t, 3H, CH_3), 4.51 (m, 2H, CH_2), 4.77 (s, 2H, CH_2), 7.31 (t, 1H), 7.55 (t, 1H), 7.70-7.84 (m, 3H), 8.08 (s, 1H), 8.30 (d, 1H), 8.51 (s, 1H). Elem. Anal. Calcd. for $C_{20}H_{16}N_2O_3S_2$: C, 60.59%; H, 4.07%; N, 7.07%; S, 16.18%. Found: C, 60.34%; H, 4.15%; N, 6.88%; S, 15.97%.

Preparation of Dye-Sensitized TiO_2 Electrode (photoanode) and Counter Electrode

F-doped tin oxide (FTO) glass plates (3 mm thickness, 7 Ω cm^{-2}) were first cleaned ultrasonically in a cleaning detergent solution for 15 min, and rinsed with water and ethanol. The FTO electrodes were then immersed into 40 mM $TiCl_4$ (aqueous) at 70 °C for 30 min and rinsed with water and ethanol. Two kinds of TiO_2 paste, containing nanocrystalline (~25 nm) TiO_2 (Degussa P25, paste A) and submicroparticle TiO_2 (500 nm, paste B), respectively, were prepared using a previously reported procedure [18,19]. To prepare paste A, commercial titania powder (3 g, Degussa P25) was ground in a mortar with a small amount of water (1 ml) containing acetylacetone (0.1 ml). After the TiO_2 particles were dispersed, the paste was diluted with 3 ml water under continued

grinding and a surfactant, Triton X-100 (0.05 ml), was added to facilitate the spreading of the colloid on the substrate. Paste A was sonicated for about 24 h at 28 °C. TiO_2 film (12 μm) was prepared by spin coating. After paste A was dried at 125 ^oC, ~4 μm thick paste B was spin-coated on top of it. The electrodes coated with TiO_2 pastes were gradually heated (5 °C min^{-1}) under airflow up to 450 °C for 30 min followed by treating with 40 mM $TiCl_4$, rinsed with water and ethanol, and sintered again at 450 °C for 30 min. The electrodes with an active area of 0.5 cm × 0.5 cm were immersed in a 1:1 acetonitrile and isoporpanol solution containing 3×10^{-4} M of the dye. The dye-adsorbed TiO_2 films were then rinsed with dry ethanol, and dried in air. A counter electrode was prepared by sputtering a thin platinum layer (50 nm) on an FTO substrate. The thicknesses of the TiO_2 films were determined by profilometry. Platinum sputtering was carried out using a Hitachi E 1045 instrument. The platinum layer thickness on the glass substrates was estimated using the amount of sputtered platinum recorded on a quartz thickness monitor.

DSSC Assembly

The dye-adsorbed TiO_2 electrode and Pt-counter electrode were assembled into a sandwich-sealed type cell by heating them with hot-melt ionomer film (25 μm thickness, Solaronix) as a spacer. A drop of electrolyte solution: 0.1 M LiI, 0.05 M I_2, 0.6 M DMPII and 0.5 M tert-butyl pyridine (TBP) in acetonitile (ACN)) was injected through a hole in the counter electrode, which was then sealed with hot-melt ionomer film and glass. The electrolyte was introduced into the cell and sealed with AB epoxy for 30 min. The working area of the electrode was 0.25 cm^2.

Characterization of the Dyes and Photovoltaic Measurements of the Solar Cells

The ^1H spectra were obtained on a Bruker 400 MHz FT-NMR. Chemical shifts are reported in ppm relative to tetramethylsilane δ units. The absorption spectra of the dyes in solution and adsorbed on TiO_2 films were recorded on a Cary 100 UV-Vis spectrophotometer. Fluorescence measurements were carried out using a Hitachi F-4500 fluorescence spectrophotometer. Cyclic voltammetry was performed using an electrochemical workstation (CH instruments Inc., CHI, model 750A) and conducted in CH_3CN solution using 0.1 M tetrabutylammonium perchlorate (TBAP) as the supporting electrolyte. The working electrode was a glassy carbon electrode, the auxillary electrode was a Pt wire, and the reference electrode was Ag/Ag^+. The scan rate was 100 mV s^{-1} and the temperature was 25 °C. Ferrocene was added to each sample solution at the end of the experiments. The ferrocenium/ferrocene (Fc/Fc^+) redox couple was used as an internal potential reference. The potential versus SCE in acetonitrile was calibrated according to a procedure published by Matsui *et al*. [20]. The photovoltaic measurements of the DSSCs were performed using a Newport M-66907 450 W xenon light source through an infrared blocking filter and a Keithley 2400 digital source meter linked to a computerized control and data acquisition system. The light intensity was 1000 W m^{-2} under an AM 1.5 light source. Cell temperatures were kept at 25 °C during the illumination. Light intensity was calibrated using a mono-Si reference solar cell (PVM134). The incident photon-to-current conversion efficiency (IPCE) as a function of excitation wavelength was measured using an incident light 300 W xenon lamp. A 300W xenon arc lamp solar simulator (#91160A, Oriel) with an AM 1.5 Globe filter (#59044, Oriel) was used to measure the I-V characteristics of the quasi-solid-state DSSC. The illumination was fixed at 100 mW cm^{-2} using a reference solar cell and meter (#91150, Oriel).

Computation Methods

R1-**R3** are the carbazole, iminodibenzyl, and phenothiazine-containing dyes, respectively. The geometric and electronic properties of **R1**-**R3** were obtained using the Gaussian 03 program package [21]. The calculation was optimized using B3LYP (Becke three parameter hybrid function with Lee-Yang-Perdew correlation functions) with the Pople 6-31+g(d) atomic basis set. The excitation transitions of **R1**, **R2**, and **R3** were calculated using time-dependent density functional theory (TD-DFT) calculations with B3LYP/6-31+g(d). Molecular orbitals were visualized using Gaussview.

RESULT AND DISCUSSION

Synthesis and Structure of Sensitizers

In this study, three donor-acceptor π-conjugated dyes with

a carboxyl group were synthesized; the amine derivatives acted as the electron donors while a rhodanine-3-acetic acid moiety acted as the anchoring group for attachment on the metal oxide and as the electron acceptor. The two components were connected by a π-conjugated methane unit. The electron-donating nature and structural variations of the amine unit and its electronic properties were studied.

As is shown in Fig. 1, **R1**-**R3** are the carbazole, iminodibenzyl, and phenothiazine-containing dyes, respectively. The aldehydes (**3a**, **3b**, **3c**) were prepared by treating *N*-ethylcarbazole, *N*-ethyliminodibenzyl, and *N*-ethylphenothiazine with $POCl_3$ in DMF as previously reported by Lai *et al*. [22]. The final reaction for **R1**, **R2**, and **R3** was the condensation of the respective aldehyde with rhodanine-3-acetic acid by the Knoevenagel reaction in the presence of ammonium acetate. The optimized structures of **R1**, **R2** and **R3** were studied to compare the structure differences between carbazole, iminodibenzyl, and whereas the dihedral angle between the phenyl unit and dimethylene bridge inside the iminodibenzyl unit (∠4) was 126°. This could be attributed to the incorporation of a dimethylene bridge between two phenyl units increasing the steric hindrance, increasing the dihedral angles of ∠1 and ∠4. Dihedral angles may affect the stability and suitability of dyes as photosensitizers. Planar carbazole unit readily causes intermolecular π-π stacking interactions. The incorporation of dimethylene bridge and sulfur units to iminodibenzyl and phenothiazine-based photosensitizer (**R2** and **R3**), respectively, reduces the coplanarity of photosensitizers, and minimizes the formation of dye aggregates on the semiconductor surface. The dihedral angle (∠5) of the **R3** phenothiazine sulfur atom is 99.2°, which is smaller than that of the phenothiazine nitrogen atom (∠1: 122.1°). This may be attributed to the structure difference between nitrogen and sulfur atoms; nitrogen atom has a lone pair whereas sulfur atom has two lone pairs.

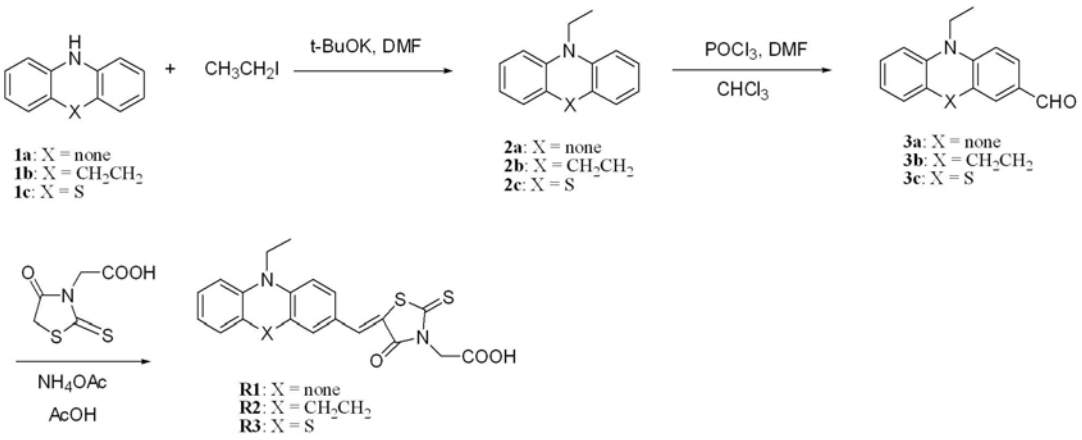

Fig. 1. Synthesis of the carbazole, iminodibenzyl and phenothiazine substituted dyes.

phenothiazine photosensitizers (Fig. 2). The dihedral angles (∠1) of the **R1** carbazole ring, the **R2** iminodibenzyl ring, and the **R3** phenothiazine ring were 108.7°, 123.7°, and 122.1°, respectively, implying that the addition of a dimethylene bridge and sulfur units significantly increases the dihedral angle of nitrogen atoms. The dihedral angle between two phenyl units inside the carbazole unit (∠4) was 106.4°;

Optical Properties

The UV-Vis and emission spectra of **R1**, **R2**, and **R3** in CH_3CN are shown in Fig. 3 and the λ_{max} are listed in Table 1, together with the UV-Vis spectra of the corresponding dyes adsorbed on TiO_2 film. All dyes show broad absorption spectra ranging from 350 to 800 nm. The absorption spectrum of **R1** in CH_3CN has two distinct absorption bands at around

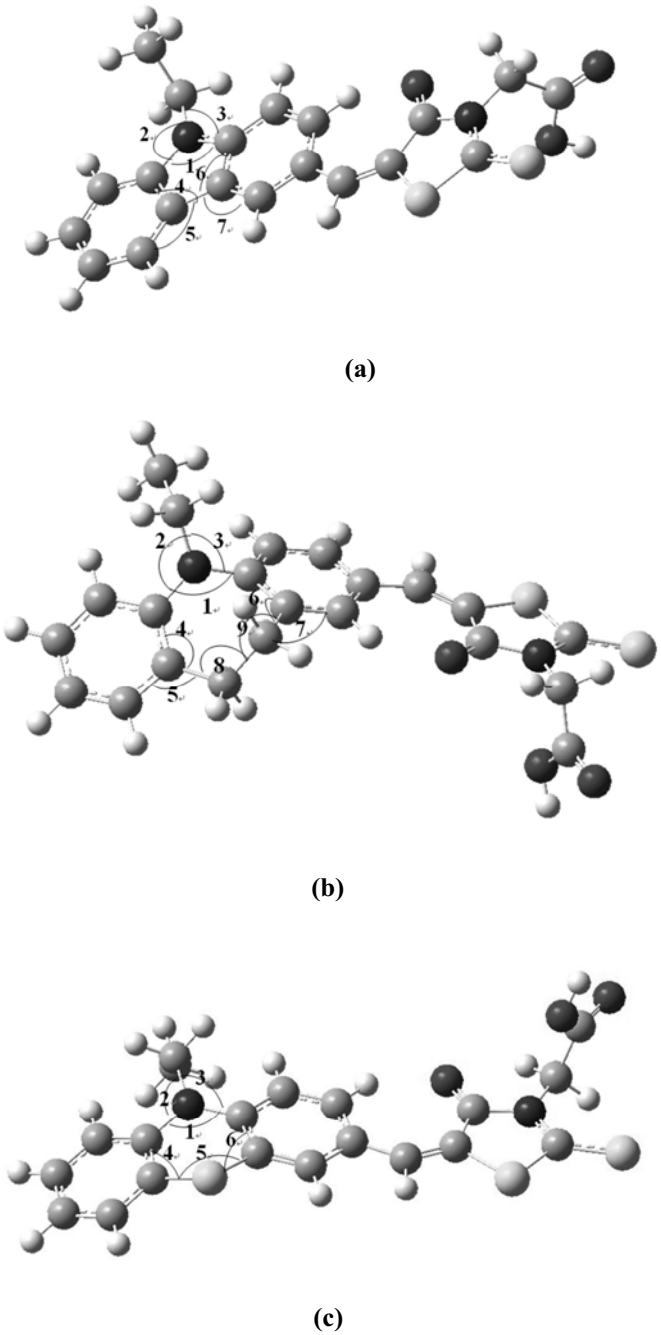

Fig. 2. Optimized geometric parameters (dihedral angle) of (a) **R1**: ∠1 = 108.7°, ∠2 = 125.4°, ∠3 = 125.8°, ∠4 = 106.4°, ∠5 = 134.0°, ∠6 = 106.6°, ∠7 = 134.0°; (b) **R2**: ∠1 = 123.7°, ∠2 = 119.0°, 3 = 117.2°, ∠4 = 126°, ∠5 = 115.9°, ∠6 = 119.1°, ∠7 = 120.9°; ∠8 = 116.4°, ∠9 = 111° and (c) **R3**: ∠1 = 122.1°, ∠2 = 118.4°, ∠3 = 118.7°, ∠4 = 120.6°, ∠5 = 99.2°, ∠6 = 120.4°.

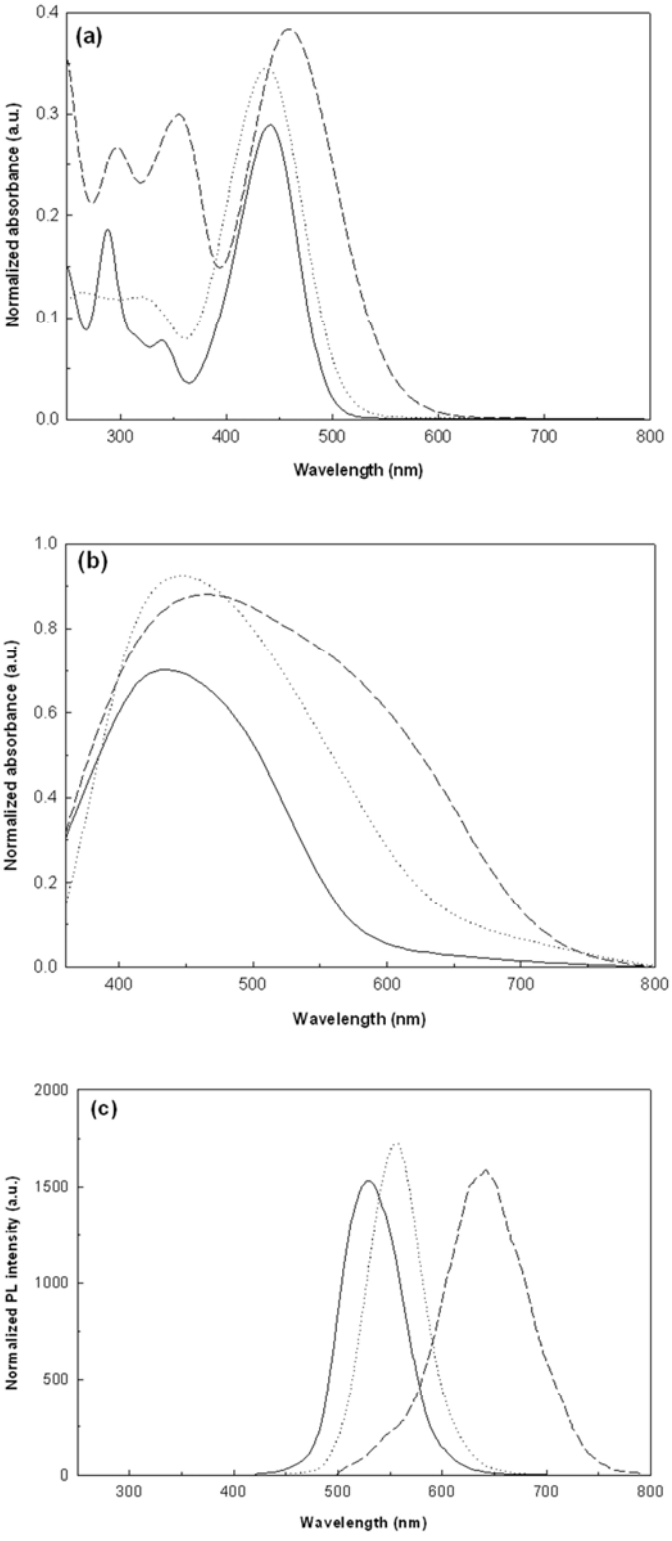

Fig. 3. Absorption spectra of **R1** (—), **R2** (…), and **R3** (---) (a) in CH_3CN and (b) absorption on TiO_2 film. (c) Emission spectra of **R1** (—), **R2** (…), and **R3** (---).

Table 1. Absorption and Emission Properties of Dyes

Dye	Absorption			Emission	Stokes shift
	λ_{abs} (nm)[b]	ε (M^{-1} cm^{-1}) (at λ_{abs})	λ_{abs} (nm)[b] (on TiO_2)	λ_{em} (nm)[b]	(nm)[a]
R1[b]	288, 442	22260 (442 nm)	445	531	89
R2	438	26583 (438 nm)	449	556	118
R3	298, 356, 460	29521 (460 nm)	469	642	182

[a]Stokes shift = $PL_{(soluion)}$/nm - $UV_{(solution)}$/nm. [b]Absorption and emission spectra were measured in CH_3CN solution.

288 and 442 nm, respectively. The weak absorption peaks at around 288 nm correspond to the π→π* electron transition of the conjugated molecule; the strong absorption peaks at around 442 nm can be assigned to an intramolecular charge transfer between the carbazole-based donor and the rhodanine-3-acetic acid [3], providing efficient charge-separation at the excited state. Under similar conditions, the **R2** sensitizer had absorbance peak at 438 nm representing a slight hypsochromic shift relative to that of **R1**, implying that the incorporation of dimethylene bridge interrupts the conjugation between two phenyl groups.

Comparing the maximum absorption wavelength of **R1**-**R3** in CH_3CN solution, **R3** (460 nm) shows significant red shift relative to **R1** (442 nm) and **R2** (438 nm) which can be attributed to the extra electron-donating sulfur atom in **R3**. Red-shifting in the absorption spectra helps the utilization of solar light. When the **R1** sensitizer was adsorbed on the TiO_2 surface, there was a slight red shift from 442 to 445 nm (Table 1), implying that dyes adsorbed on the TiO_2 surface had partial J-type aggregates. However, the stronger red shift of **R2** (438 nm → 449 nm) compared to that of **R1** (442 → 445 nm) from the solution to TiO_2 film could imply that the iminodibenzyl-containing sensitizer had a higher tendency to form surface binding with TiO_2 than that of carbazole-containing sensitizer, as chelating to metal cation, it may enhance the intramolecular electron transfer (ICT), leading to spectrum shift. Under similar conditions, the **R3** sensitizer showed a slight red shift from 460 to 469 nm after being adsorbed on the TiO_2 surface.

The absorption spectra of **R1-R3** on the TiO_2 electrode are broader than those in CH_3CN. The broadening of the absorption spectra is due to an interaction between the dyes and TiO_2 [23-24]. The absorption redshift of **R3** relative to **R2** is due to its stronger intramolecular charge transfer because phenothiazine is a stronger electron-donating ring than iminodibenzyl. The molar extinction coefficients of **R1**, **R2**, and **R3** are 22260 M^{-1} cm^{-1} (at 442 nm), 26583 M^{-1} cm^{-1} (at 438 nm), and 29521 M^{-1} cm^{-1} (at 460 nm), respectively; they are larger than that of **N3** (*cis*-bis(isothiocyanato)bis(2,2'-bipyridyl-4,4'-dicarboxylato)-ruthenium(II)) (14200 M^{-1} cm^{-1}) [25], indicating that the novel dyes have good light harvesting ability.

As is shown in Fig. 3c, the PL (photoluminescence) maximum of **R1** is located at 531 nm in CH_3CN, whereas that of **R2** shifted to 556 nm, and that of **R3** shifted to 642 nm. **R3** exhibited a relatively large Stokes shift, which could be attributed to the geometrically relaxed structure of the phenothiazine center upon excitation [26].

Electrochemical Properties

Cyclic voltammetry was used to determine the redox potentials of the dyes in order to estimate the driving force of the photoinduced electron injection process. To determine the possibility of electron transfer from the excited dye molecules to the conduction band of the TiO_2 electrode, redox potentials of **R1**, **R2**, and **R3** were obtained using cyclic voltammetry. The HOMO energy level was estimated by using the onset anodic potentials E_{ox} (*vs*. NHE). The LUMO energy level was calculated by "E_{ox}-$E_{0\text{-}0}$", where $E_{0\text{-}0}$ is determined from the intersection of absorption and emission spectra.

Usually, the energy level of the ground state ($E^0_{D^+/D}$) is estimated from its equilibrium redox potential (E_{ox}). The ferrocenium/ferrocene (Fc/Fc^+) redox couple was used as an internal potential reference. Figure 4 shows the cyclic voltamograms of **R1**, **R2**, and **R3** in acetonitrile. The

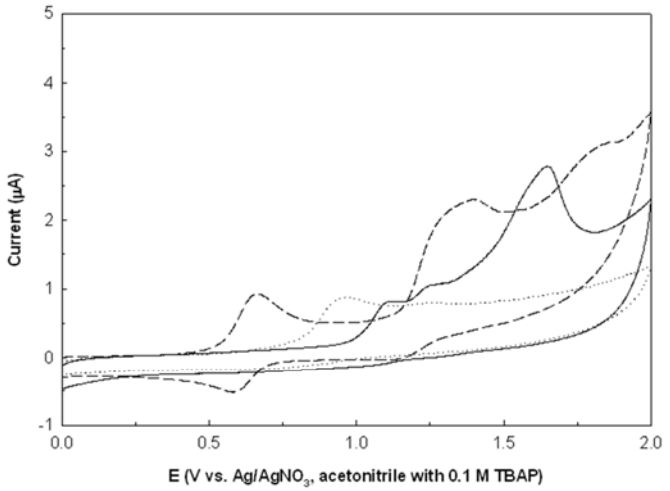

Fig. 4. Cyclic voltamogram of **R1** (—), **R2** (…), and **R3** (---) in acetonitrile.

electrochemical data are listed in Table 2. When **R1** was swept in the anodic direction, there was an obvious oxidation peak at 1.66 V, and two small oxidation peaks at 1.12, 1.25 V. However, there was no reduction peak, indicating that the electrochemical behavior in the anodic direction was irreversible. For **R2**, the oxidation was also irreversible, with peak appearing at 0.96 V. The $E_{onset\ (ox)}$ and the oxidation peak of **R2** were lower than those of **R1**, which could be attributed to the relatively higher electron density on the nitrogen atoms of **R2**, allowing it to be more easily oxidized than carbazole derivatives. It is evident that the iminodibenzyl unit enhanced the hole transporting ability of the photosensitizer than that of carbazole unit. The first oxidation peak of **R3** (0.68 V) was a reversible one electron reaction. Both the $E_{onset\ (ox)}$ and the first oxidation potentials of **R3** were less positive than those of **R2**, indicating that the phenothiazine units were much more effective in lowering the ionization potential than iminodibenzyl units. Moreover, introducing a phenothiazine group into the photosensitizer framework (**R3**) resulted in a largely negative shift of the HOMO level, to 0.52 V *vs*. NHE. The HOMO levels of **R1** and **R2** (1.01 and 0.85 V *vs*. NHE, respectively) were more positive than that of **R3**, indicating more efficient dye regeneration for **R1** and **R2**. The LUMO level of **R3** (-1.74 V *vs*. NHE) was more negative than those of **R1** and **R2** (-1.54 and -1.61 V *vs*. NHE, respectively), indicating that **R3** dye had more efficient electron injection.

Figure 5 shows the schematic energy diagram of these dye-sensitized TiO_2 electrodes. All the excited state oxidation potentials (LUMO) of **R1** (-1.54 V), **R2** (-1.61 V), and **R3** (-1.74 V) were more negative than the conduction band edge of TiO_2 (-0.5 V (*vs*. NHE)) [27]. Provided that an energy gap (between dye LUMO and TiO_2 CB) of 0.2 eV is necessary for efficient electron injection [28], the driving force is sufficient for efficient charge injection. Thus, the electron injection process from the excited dye molecule to the TiO_2 conduction band and the subsequent dye regeneration are energetically permitted. Figure 5 also indicates that the energy levels of the ground state (HOMO) of **R1** (1.01 V), **R2** (0.85 V), and **R3** (0.52 V) are sufficiently more positive than the I_3^-/I^- redox potential (0.42 V (*vs*. NHE)) [27], indicating that the oxidized

Table 2. Electrochemical Properties and Band Gaps of **R1~R3** Dyes

Dye	E_{pa}	$E_{onset(ox)}$ measured in CH_3CN	$E_{onset(ox)}$ *vs*. E_{FOC} (V)[a]	$E(S^+/S^*)$ (V)[b,d] *vs*. NHE	$E_{0\text{-}0}$ (eV) [c]	LUMO *vs*. NHE (eV)	E_{gap} (V)[e]
R1	1.12, 1.25, 1.66	0.98	0.72	1.01	2.55	-1.54	1.04
R2	0.96	0.82	0.56	0.85	2.46	-1.61	1.11
R3	0.68, 1.4, 1.86	0.49	0.23	0.52	2.26	-1.74	1.24

[a]E_{FOC} = 0.26 V *vs*. Ag/Ag^+. [b]The ground-state oxidation potentials $E(S^+/S)$ were measured in acetronitrile containing 0.1 M tetrabutylammonium perchlorate as supporting electrolyte using a glassy carbon working electrode, a Pt counter electrode, and a Ag/Ag^+ reference electrode. [c]The $E_{0\text{-}0}$ value was estimated from the cross-section of absorption and emission spectra. [d]The excited-state oxidation potential $E(S^+/S^*)$ was calculated from $E(S^+/S)$ - $E_{0\text{-}0}$. [e]E_{gap} is the energy gap between $E(S^+/S^*)$ of the dye and the conduction band level of TiO_2 (-0.5V *vs*. NHE).

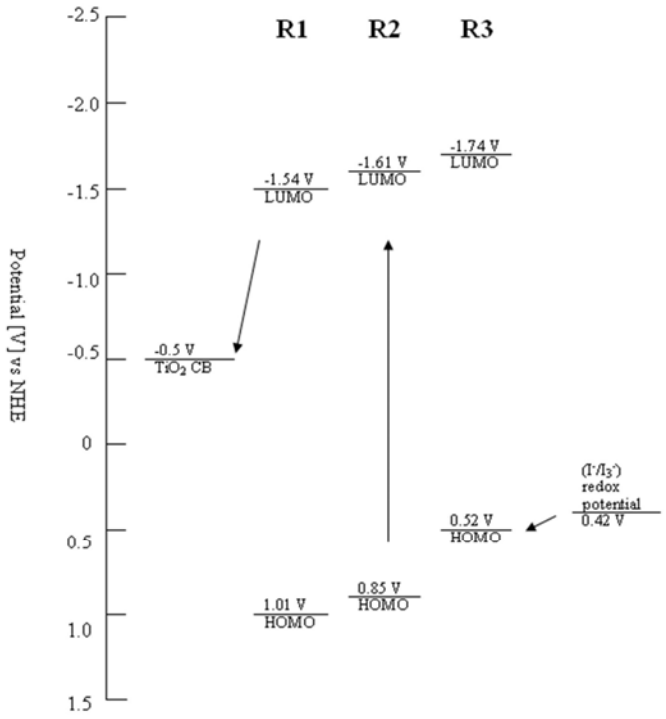

Fig. 5. Schematic energy level diagram for a DSSC based on dyes.

dye formed after electron injection into the conduction band of TiO_2 could accept electrons from I^- ions in the electrolyte thermodynamically. Therefore, these dyes could be candidates for sensitizers in DSSCs.

Molecular Orbital Calculations

The geometries of the organic dyes were optimized using density functional theory (DFT) calculations at a B3LYP/6-31+G (D) level, as shown in Fig. 6. The frontier MOs of **R1**-**R2** reveal that HOMO-LUMO excitation moves the electron density distribution from the carbazole and iminodibenzyl moiety to the rhodanine-3-acetic acid moiety; however, the frontier MOs of **R3** reveal that the electrons at the ground state (HOMO) are homogeneously distributed in both the electron donor group and the methylene bridge and rhodanine-3-acetic acid moiety. Comparing the frontier MOs of **R1** and **R2** at the ground state (HOMO), the electrons of **R2** are dominantly distributed in the benzene ring and the nitrogen atom; however, there are few electrons in the dimethylene bridge of the iminodibenzyl unit. The electrons of **R3** are homogeneously distributed in the phenothiazine unit. The LUMO electron density geometry distributions of **R1**-**R3** are located over the rhodanine-3-acetic acid group through the right phenyl group and the nitrogen atom of carbazole, iminodibenzyl and phenothiazine units, respectively. At the excited state (LUMO) with light illumination for **R1**-**R3** dyes, intramolecular charge transfer occurs, resulting in electron movement from the donor group to the acceptor groups (rhodanine-3-acetic acid group). Furthermore, the location of the LUMO at the side of the TiO_2 surface and the HOMO at the opposite end of the molecule make the electron injection into the semiconductor easier and prevent back regeneration of the dye with the injected electrons.

We modelled the electronic structure of sensitizers both in vacuo and in CH_3CN solution. It was found that the inclusion of solvation effects did not lead to a qualitative change in the electronic structure, even though smaller HOMO-LUMO gaps were calculated in CH_3CN as compared to the gas phase. The

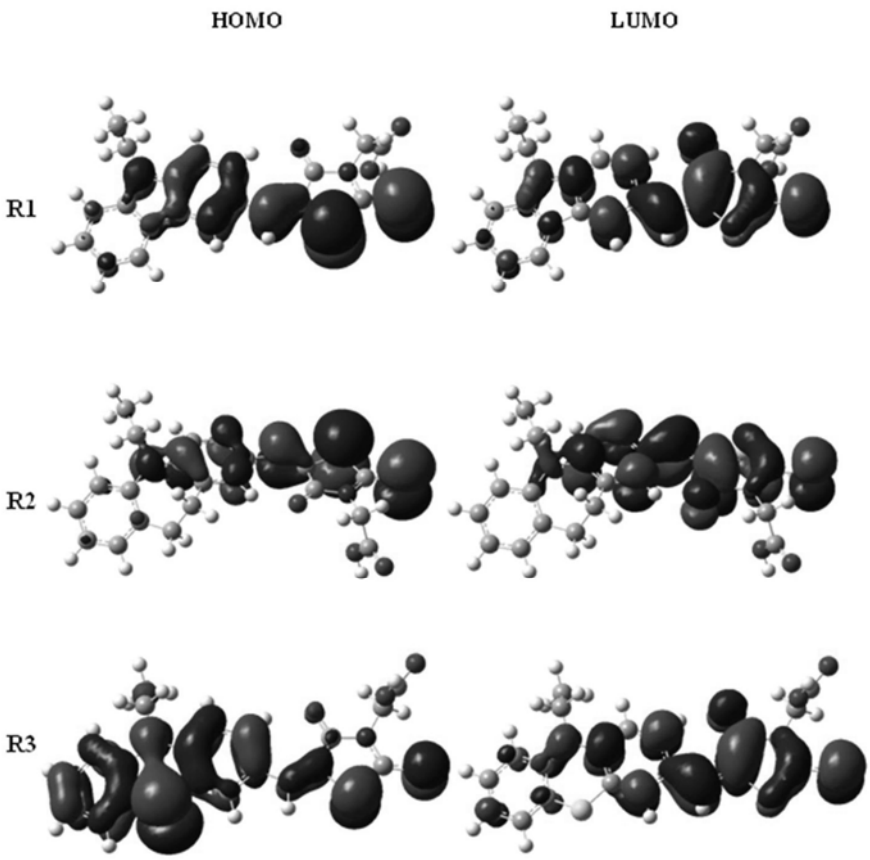

Fig. 6. Computed isodensity surfaces of HOMO and LUMO orbitals of **R1**, **R2**, and **R3**.

origins of these electronic absorptions were found by calculating the singlet electronic transitions with the TDDFT method in Gaussian 03W program suite. Calculations show that these visible bands are mainly attributed to the electronic transition from the highest occupied molecular orbitals (HOMOs) to the lowest unoccupied molecular orbitals (LUMOs). Table 3 shows the calculated absorption maxima in the visible region, their oscillator strengths, and their compositions for **R1**-**R3**. To analyze the photophysical properties of these dyes, we performed TD-DFT calculations of the lowest 10 singlet-singlet excitations of dyes in CH_3CN solutions. The three transitions of **R1**-**R3** with oscillator strengths (*f*) above 0.05 are summarized in Table 3. Compared with the experimental data, the considerable blue-shift of the absorption maximum from the calculations is related to the self-interaction error in TD-DFT arising from the electron transfer in the extended charge-transfer state [29]. The calculated absorption maxima for the excited states seem to be in good agreement with the measured values, supporting the band assignments in the UV solution plot.

Photovoltaic Performance

DSSCs were prepared and compared to investigate the relationships between the sensitizing behavior of **R1-R3** dye molecules and their structures. The incident photon-to-current conversion efficiency (IPCE) of a DSSC was estimated to be between 400 and 800 nm. The IPCE values were measured according to the following equation [30]:

$$\mathrm{IPCE}(\lambda) = \frac{1240(\mathrm{eV}\cdot\mathrm{nm})}{\lambda(\mathrm{nm})}\frac{Jsc(\mathrm{mA}\cdot\mathrm{cm}^{-2})}{\phi(\mathrm{mW}\cdot\mathrm{cm}^{-2})}$$

where λ is the wavelength and ϕ is the power of the incident

Table 3. Comparison of Calculated TD-DFT Excitation Energies (eV, nm), Oscillator Strengths (*f*), Assignment of Molecular Orbital Contributions and Character, and Experimental Absorption Band Maxima of Dyes

Dye	Excited state	f	Est (eV)	Est (nm)	Exp (eV)	Exp (nm)	Composition
R1	1	0.9156	2.7072	457.97	2.81	442	0.65135χ(HOMO → LUMO)
	2	0.2068	3.5985	344.55			0.65219χ(HOMO-2 → LUMO) -0.10005χ(HOMO-1 → LUMO+2) +0.11737χ(HOMO → LUMO+2)
	3	0.1195	4.2929	288.81	4.31	288	0.54447χ(HOMO-5 → LUMO) +0.32952χ(HOMO-4 → LUMO) +0.12395χ(HOMO-1 → LUMO+2) -0.11414χ(HOMO → LUMO+1)
R2	1	0.7783	3.1809	389.78	2.83	438	0.64708χ(HOMO-1 → LUMO)
	2	0.2756	2.2543	549.98			0.68084χ(HOMO → LUMO)
	3	0.1113	4.1741	297.03			0.13954χ(HOMO-7 → LUMO) +0.59457χ(HOMO-6 → LUMO) -0.21827 (HMOM-5 → LUMO) -0.18699χ(HOMO-1 → LUMO+1)
R3	1	0.5985	3.1452	394.2	2.70	460	0.11165χ(HOMO-2 → LUMO) +0.65586χ(HOMO-1 → LUMO)
	2	0.1053	3.5465	349.6	3.49	356	0.63479χ (HOMO-2 → LUMO) +0.16037χ(HOMO → LUMO+2)
	3	0.0686	4.1977	295.36	4.16	298	-0.11214χ(HOMO-7 → LUMO) +0.29511χ(HOMO-6 → LUMO) +0.41153 (HOMO-5 → LUMO) -0.23046χ(HOMO-4 → LUMO) -0.21544χ(HOMO-1 → LUMO+1) +0.14252χ(HOMO → LUMO+2) +0.23590χ(HOMO → LUMO+3) +0.10978χ(HOMO → LUMO+4)

radiation per unit area.

Figure 7 shows action spectra of monochromatic incident-to current conversion efficiencies (IPCEs) for DSSCs using **R1**-**R3**. The IPCEs of **R1**, **R2**, and **R3** are 43-58% in the spectral range from 460 to 520 nm, and **R3** reaches its maximum of 58% at 500 nm. When reflection and absorption losses of the FTO glass substrate are considered, the net photon-to-electron conversion efficiencies of the three dyes (**R1**, **R2**, and **R3**) would almost exceed 60% in their spectral ranges. The decrease of the IPCE above 750 nm in the long-wavelength region is attributed to the decrease of light harvesting for these dyes.

A typical photocurrent-photovoltage (*I-V*) curve for cells based on **R1**, **R2**, and **R3** is shown in Fig. 8. The detailed photovoltaic parameters are summarized in Table 4. The solar-energy-to-electricity conversion efficiency (η) of the DSSCs is calculated from short-circuit current (J_{sc}), the open-circuit photovoltage (V_{oc}), the fill factor (FF), and the intensity of the incident light (P_{in}) according to the following equation [30]:

$$\eta = \frac{[J_{sc}(\mathrm{mA\cdot cm^{-2}})][V_{oc}(\mathrm{V})][\mathrm{FF}]}{P_{in}(\mathrm{mW\cdot cm^{-2}})}$$

Under the standard global AM 1.5 solar condition, the **R1** cell had a J_{sc} of 6.62 mA cm^{-2}, V_{oc} of 587 mV, and a fill factor of 0.65, corresponding to an overall conversion efficiency of 2.54%. Under similar conditions, the photovoltaic parameters (J_{sc}, V_{oc} and η) of cells with the **R2** sensitizer were 7.46 mA cm^{-2}, 625 mV, and 3.52%, respectively, and those of the **R3**

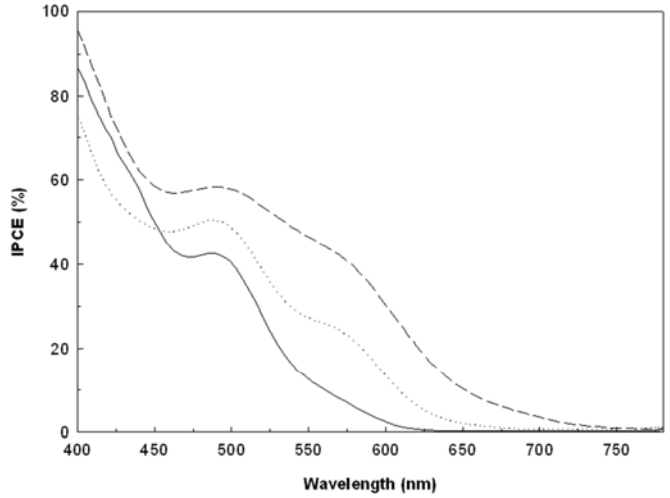

Fig. 7. The incident photon-to-current conversion efficiency spectra for DSSCs based on **R1** (—), **R2** (…), and **R3** (---).

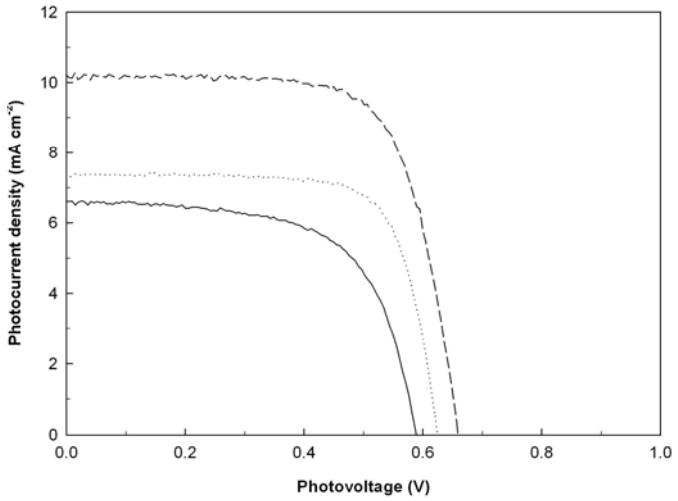

Fig. 8. Current density-voltage characteristics for **R1** (—), **R2** (…), and **R3** (---) DSSCs under illumination of simulated solar light (AM 1.5, 100 mW cm^{-2}).

sensitizer were 10.34 mA cm^{-2}, 661 mV, and 4.87%, respectively. The greater efficiency of the **R3** sensitizer is probably due to the strong electron-donating ability of the phenothiazine unit when electrons transfer from the phenothiazine unit to the rhodanine-3-acetic acid group. A large *V*oc is also a prerequisite for higher power conversion efficiencies of phenothiazine substituted dyes.

Table 4. Photovoltaic Performance of DSSCs Based on **R1**, **R2**, and **R3** Dyes

Dye	V_{oc} (mV)	J_{sc} (mA cm^{-2})	Fill factor (ff)	η (%)
R1	587.27	6.62	0.65	2.54
R2	624.95	7.46	0.75	3.52
R3	660.55	10.34	0.71	4.87

[a]Measured under irradiation of AM 1.5 G simulated solar light (100 mW cm^{-2}) at room temperature, 10 μm film thickness, 0.25 cm^2 working area. [b]The concentration of dye is 2×10^{-4} M in CH_3CN and 0.6 M tetrabutylammonium iodide (TBAI), 0.1 M LiI, 0.05 M I_2, 0.6 M DMPII, and 0.5 M 4-tert-butylpyridine (TBP) in dry acetonitrile (ACN) as electrolyte.

Mechanism of Photon-to-Current Conversion in the DSSCs

Figure 9 shows the schematic energy diagram for a DSSC based on the **R2** photosensitizer. A thin film of electrolyte solution (I^-/I_3^- dissolved in an organic solvent) is sandwiched between the TiO_2 electrode and another transparent conducting electrode (counter electrode). The **R2** photosensitizer is attached to very small particles (nanocrystalline structure) of titanium dioxide where it acts as a light absorber. Based on the electrochemical properties and photocurrent-voltage characteristics, the relevant electron-transfer process for the **R2** sensitized TiO_2 electrode involves the following processes. First, the dye is excited from the ground state to the excited state by the absorption of incident photon flux due to the intramolecular π-π* transition. Second, the excited electrons are injected into the conduction band of the TiO_2 electrode immediately before quenching by emission and consequent formation of the oxidized dye. Third, the injected electrons in the conduction band of TiO_2 are transported toward the Pt counter electrode through the external load. Fourth, the iodide is regenerated by the reduction of triiodide at the Pt counter electrode. Finally, the oxidized dyes are reduced to the ground state by accepting electrons from iodide anions that have been oxidized to triiodide anions. The process leads to photovoltaic

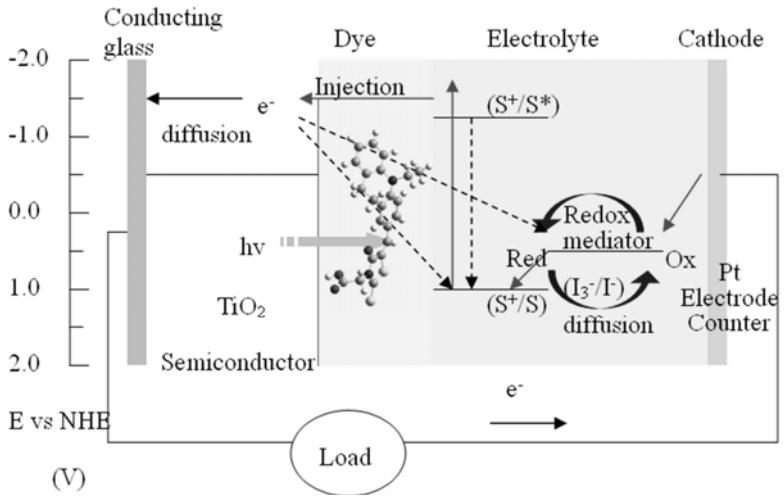

Fig. 9. Schematic energy diagram for a DSSC based on the **R2** photosensitizer, I^-/I_3^- redox electrolyte, TiO_2 anode, and Pt cathode.

performance in the solar cell.

CONCLUSIONS

Three dyes containing carbazole, iminodibenzyl, and phenothiazine units, respectively, were designed and synthesized as the sensitizers for DSSCs applications. Iminodibenzyl is a diphenylamine wherein two *ortho* positions are joined by a dimethylene bridge. Phenothiazine sensitizer contains extra electron-donating sulfur in addition to nitrogen. The optical, electrochemical, and photovoltaic performances were affected by structural modifications. The LUMO values of **R1** (-1.54 V), **R2** (-1.61 V), and **R3** (-1.74 V) are more negative than the conduction band edge of TiO_2 (-0.5 V (*vs*. NHE)). The HOMO values of **R1** (1.01 V), **R2** (0.85 V), and **R3** (0.52 V) were sufficiently more positive than the I_3^-/I^- redox potential (0.42 V (*vs*. NHE)). The density functional theory (DFT) calculations revealed that HOMO-LUMO excitation moved the electron density distribution from the donor to the acceptor (rhodanine-3-acetic acid). The DSSCs based on the **R3** dye showed the best photovoltaic performance: a maximum monochromatic incident photon-to-current conversion efficiency (IPCE) of 58%, a short-circuit photocurrent density (J_{sc}) of 10.34 mA cm^{-2}, an open-circuit photovoltage (V_{oc}) of 661 mV, and a fill factor (ff) of 0.71, corresponding to an overall conversion efficiency of 4.87% under 100 mW cm^{-2} irradiation. Accordingly, dyes based on carbazole, iminodibenzyl and phenothiazines are promising candidates for DSSCs.

ACKNOWLEDGEMENTS

The authors would like to thank the National Science Council of the Republic of China for financially supporting this project under grant: 96-2113-M-006-014-MY3.

REFERENCES

[1] B. O'Regan, M. Grätzel, Nature 353 (1991) 737.

[2] P. Wang, S.M. Zakeeruddin, J.E. Moser, M.K. Nazeeruddin, T. Sekiguchi, M. Grätzel, Nat. Mater. 2 (2003) 402.

[3] M. Liang, W. Xu, F. Cai, P. Chen, B. Peng, J. Chen, Z. Li, J. Phys. Chem. C 111 (2007) 4465.

[4] V. Mirkhani, S. Tangestaninejad, M. Moghadam, M.H. Habibi, A. Rostami-Vartooni, J. Iran. Chem. Soc. 6 (2009) 578.

[5] A. Kumar, M. Paliwal, R. Ameta, S.C. Ameta, J. Iran. Chem. Soc. 5 (2008) 346.

[6] J. Saien, A.R. Soleymani, J. Iran. Chem. Soc. 6 (2009)

602.

[7] J. Kasthuri, J. Santhanalakshmi, N. Rajendiran, J. Iran. Chem. Soc. 5 (2008) 436.

[8] I. Jung, J.K. Lee, K.H. Song, K. Song, S.O. Kang, J. Ko, J. Org. Chem. 72 (2007) 3652.

[9] K. Hara, Y. Tachibana, Y. Ohga, A. Shinpo, S. Suga, K. Sayama, H. Sugihara, H. Arakawa, Sol. Energy Mater. Sol. Cells 77 (2003) 89.

[10] T. Horiuchi, H. Miura, S. Uchida, Chem. Commun. (2003) 3036.

[11] K. Sayama, S. Tsukagoshi, K. Hara, Y. Ohga, A. Shinpou, Y. Abe, S. Suga, H. Arakawa, J. Phys. Chem. B 106 (2002) 1363.

[12] Q.-H. Yao, L. Shan, F.-Y. Li, D.-D. Yin, C.-H. Huang, New J. Chem. 27 (2003) 1277.

[13] Z.G. Chen, F.Y. Li, C.H. Huang, Curr. Org. Chem. 11 (2007) 1241.

[14] K. Hara, M. Kurashige, S. Ito, A. Shinpo, S. Suga, K. Sayama, H. Arakawa, Chem. Commun. (2003) 252.

[15] S.L. Li, K.J. Jiang, K.F. Shao, L.M. Yang, Chem. Commun. (2006) 2792.

[16] K. Hara, T. Sato, R. Katoh, A. Furube, Y. Ohga, A. Shinpo, S. Suga, K. Sayama, H. Sugihara, H. Arakawa, J. Phys. Chem. B 107 (2003) 597.

[17] S.Y. Jang, V. Seshadri, M.S. Khil, A. Kumar, M. Marquez, P.T. Mather, G.A. Sotzing, Adv. Mater. 17 (2005) 2177.

[18] M.K. Nazeeruddin, S.M. Zakeeruddin, R. Humphry-Baker, M. Jirousek, P. Liska, N. Vlachopoulos, V. Shklover, C.H. Fischer, M. Grätzel, Inorg. Chem. 38 (1999) 6298.

[19] P. Wang, S.M. Zakeeruddin, P. Comte, R. Charvet, R. Humphry-Baker, M. Grätzel, J. Phys. Chem. B 107 (2003) 14336.

[20] M. Matsui, Y. Hashimoto, K. Funabiki, J. Jin, T. Yoshida, H. Minoura. Synth. Metals 148 (2005) 147.

[21] M.J. Frisch, G.W. Trucks, H.B. Schlegel, G.E. Scuseria, M.A. Robb, J.R. Cheeseman Jr., J.A. Montgomery, T. Vreven, K.N. Kudin, J.C. Burant, J.M. Millam, S.S. Iyengar, J. Tomasi, V. Barone, B. Mennucci, M. Cossi, G. Scalmani, N. Rega, G.A. Petersson, H. Nakatsuji, M. Hada, M. Ehara, K. Toyota, R. Fukuda, J. Hasegawa, M. Ishida, T. Nakajima, Y. Honda, O. Kitao, H. Nakai, M. Klene, X. Li, J.E. Knox, H.P. Hratchian, J.B. Cross, C. Adamo, J. Jaramillo, R. Gomperts, R.E. Stratmann, O. Yazyev, A.J. Austin, R. Cammi, C. Pomelli, J.W. Ochterski, P.Y. Ayala, K. Morokuma, G.A. Voth, P. Salvador, J.J. Dannenberg, V.G. Zakrzewski, S. Dapprich, A.D. Daniels, M.C. Strain, O. Farkas, D.K. Malick, A.D. Rabuck, K. Raghavachari, J.B. Foresman, J.V. Ortiz, Q. Cui, A.G. Baboul, S. Clifford, J. Cioslowski, B.B. Stefanov, G. Liu, A. Liashenko, P. Piskorz, I. Komaromi, R.L. Martin, D.J. Fox, T. Keith, M.A. Al-Laham, C.Y. Peng, A. Nanayakkara, M. Challacombe, P.M.W. Gill, B. Johnson, W. Chen, M.W. Wong, C. Gonzalez, J.A. Pople, Gaussian 03, Revision C.01 Gaussian, Inc., Wallingford, CT, 2004.

[22] G. Lai, X.R. Bu, J. Santos, E.A. Mintz, Synlett. (1997) 1275.

[23] K. Hara, M. Kurashige, Y. Dan-oh, C. Kasada, A. Shinpo, S. Suga, K. Sayama, H. Arakawa, New J. Chem. 27 (2003) 783.

[24] M. Velusamy, K.R. Justin Thomas, J.T. Lin, Y.-C. Hsu, K.-C. Ho, Org. Lett. 7 (2005) 1899.

[25] M.K. Nazeeruddin, A. Kay, I. Rodicio, R. Humpbry-Baker, E. Miiller, P. Liska, N. Vlachopoulos, M. Grätzel, J. Am. Chem. Soc. 115 (1993) 6382.

[26] R.Y. Lai, E.F. Fabrizio, L. Lu, S.A. Jenekhe, A.J. Bard, J. Am. Chem. Soc. 123 (2001) 9112.

[27] A. Hagfeldt, M. Grätzel, Chem. Rev. 95 (1995) 49.

[28] S. Ito, S.M. Zakeeruddin, R. Humphry-Baker, P. Liska, R. Charvet, P. Comte, M. K. Nazeeruddin, P. Péchy, M. Takata, H. Miura, S. Uchida, M. Grätzel, Adv. Mater. 18 (2006) 1202.

[29] A. Dreuw, M. Head-Gordon, J. Am. Chem. Soc. 126 (2004) 4007.

[30] G. Boschloo, A. Hagfeldt, J. Phys. Chem. B 109 (2005) 12093.